Magn Reson Mater Phy (2008) 21:131–147
DOI 10.1007/s10334-008-0107-5

RESEARCH ARTICLE

Magnetic field dependence of the distribution of NMR relaxation times in the living human brain

A. M. Oros-Peusquens · M. Laurila · N. J. Shah

Received: 3 October 2007 / Revised: 8 February 2008 / Accepted: 8 February 2008 / Published online: 13 March 2008

Abstract

Objective This study investigates the field dependence of the distribution of in vivo, whole-brain T_1 values, and its usefulness for white matter/grey matter segmentation. Results on T_1 values are presented on 12 healthy volunteers. T_2 and T_2^* distributions and their field dependence have been measured on the same cohort of volunteers. In this paper, however, only the T_2 and T_2^* results on a single volunteer are presented. The reported field dependence of T_2 and T_2^* values should, therefore, be given less weight than that of T_1 times.

Materials and methods Relaxation times were measured in vivo on 12 healthy volunteers, using three nearly identical whole-body scanners, operating at field strengths of 1.5, 3, and 4 T and employing nearly identical software platforms and very similar hardware. T_1 mapping was performed using TAPIR, a sequence based on the Look–Locker method. T_2^* mapping was performed with a multi-slice, multi-echo, gradient echo sequence. A multi-slice, multi-echo T_2 mapping sequence based on the Carr–Purcell–Meiboom–Gill (CPMG) method was used to map T_2. For each volunteer, the global distribution of T_1 relaxation times was described as the superposition of three Gaussian distributions. The field and age-dependence of the centroids and widths of the three Gaussians was investigated. The segmentation of the brain in white and grey matter was performed separately for each field strength. Using the T_1 segmentation and the fact that all maps were coregistered, we investigated the distribution of T_2 and T_2^* values separately for the white and grey matter and described them with a Gaussian distribution in each case.

Results Multi-slice quantitative maps were produced for the relaxation parameters T_1 (near whole-brain coverage with 41 slices), T_2^* (whole-brain coverage, 55 slices), and T_2 (27 slices). A clear age dependence was identified for grey matter T_1 values and correlated with similar behaviour observed in a separate study of the brain water content. The increase with field strength of the bulk white and grey matter T_1 values was well reproduced by both Bottomley's [1] and Fischer's [2] formulae, with parameters taken from the literature. The separation between the centroids was, however, either overestimated or underestimated by the two formulae. The width of the T_1 distributions was found to increase with increasing field.

Conclusions The study of the field dependence of the NMR relaxation times is expected to allow for better differentiation between regions which are structurally different, provide a better insight into the microscopic structure of the brain and the molecular substrate of its function.

Keywords Relaxation times · T_1, T_2, T_2^* · Whole-brain distribution of relaxation times · Field dependence of relaxation times · Age dependence of T_1 · 1.5 T · 3 T · 4 T · TAPIR · QUTE · SE_MC · Volume coverage · Quantitative MRI

A. M. Oros-Peusquens (✉) · M. Laurila · N. J. Shah
Institute of Medicine, MR Group, Research Centre Jülich,
52425 Jülich, Germany
e-mail: a.m.oros-peusquens@fz-juelich.de

N. J. Shah
Institute of Physics, University of Dortmund,
44221 Dortmund, Germany

Introduction

The exquisite and versatile tissue contrast of MRI is largely based on the variability of tissue relaxation times. Among the three relaxation times used most frequently (longitudinal T_1 and transverse T_2 and T_2^*), the longitudinal relaxation

time, T_1, has proven to be very useful for generating good anatomical contrast. NMR and MRI, being low sensitivity methods, greatly profit from the use of high static magnetic fields. Understandably, early predictions of T_1 convergence with increasing field [2] created doubt regarding the usefulness of high fields for in vivo imaging of the human brain. Indeed, all MR relaxation times show field dependence, but given the complexity of tissue this dependence cannot currently be calculated from first principles.

The advent of ultra-high field scanners (7 T and above) has made well-known contrast mechanisms such as T_2^* [3] and phase contrast [4] increasingly useful. However, the usefulness of, and the need for T_1 contrast does not appear to have been significantly jeopardised even at the highest fields at which in vivo human data have been acquired. Furthermore, given the increasing number of centres disposing of multi-scanner, multi-field environments, the investigation of the exact behaviour of the relaxation times in vivo, for normal as well as pathological tissue, has become more important than ever.

The microscopic origin of the NMR relaxation times [5] can, in principle, be used to investigate the environment of the water protons on a microscopic scale. In complex environments, such as living tissue, it seems difficult to assign relaxation rates to a single relaxation mechanism. The study of the field dependence of the relaxation rates (T_1 usually), however, has led to significant progress in the understanding of the molecular information conveyed by these NMR parameters [6–8]. The behaviour with field strength of the transverse relaxation rates R_2 and R_2^* and of their difference, R_2', provides equally interesting information regarding field inhomogeneities, paramagnetic impurities, and the relaxation mechanisms.

In the present paper we report on the results of a 12-volunteer study on the mapping of relaxation times at 1.5, 3 and 4 T and their field dependence. In order to achieve this aim, we employed three nearly identical whole-body scanners that differed largely only in the strength of the static magnetic field and the radio frequency (RF) coils employed. Longitudinal and transversal relaxation times were mapped in all 12 volunteers using sequences with brain coverage varying from whole-brain (T_2^* mapping, 55 slices), near whole-brain (T_1 mapping, 41 slices), and approximately half-brain coverage (T_2, 27 slices). For each volunteer, the scans at all three field strengths were performed during a restricted time interval (17 days on average, ranging between 3 days and 3 weeks), in order to minimise possible physiological variations in the relaxation times and water content of the brain tissue.

Since age-dependent accumulation of iron, as well as the age and sex influence relaxation times and brain tissue water content in healthy volunteers, it is very important to investigate relaxation times in a large enough number of volunteers so that different contributions can be discriminated from their field dependence.

This study builds upon a number of previous studies from our laboratory which concentrated on fast and accurate methods for T_1 and T_2^* mapping [9–15], as well as precise measurements of the quantitative water content in healthy and diseased brain tissue. In subsequent studies the influence of factors such as age, sex, and severity of disease (hepatic encephalopathy) has been investigated. The previous studies were carried out at 1.5 T, achieving a precision of 2% or better in the determination of water content and 1.5% or better for T_1 [12,13]. The methodology can, therefore, be considered as well-established, and thus only a short subsection of this paper is dedicated to validation at 3 and 4 T.

The paper concentrates on T_1, the characteristics of its distribution in the near whole-brain white and grey matter, and the way these characteristics change with the field strength. Similar features of the transversal relaxation times T_2 and T_2^* have been measured on all volunteers but are exemplified in this paper for one volunteer only. The full results regarding transversal relaxation times will be the subject of a forthcoming publication. The age dependence of the longitudinal relaxation time is investigated at different fields.

Materials and methods

Subjects

Twelve healthy volunteers were enrolled in this study. The group included both male (8) and female (4) volunteers, with ages ranging between 23 and 54 years (average age 34 (SD 9) years). The applicability of the method in vivo was checked using data acquired on one volunteer, who was scanned at all three fields over a period of 2 days. Following phantom validation studies and parameter optimisation, the group of 12 volunteers was scanned at all three fields over a period of one month. The average interval during which the three scans were performed on any given volunteer amounted to 17 (SD 10) days. During each scanning session, the subjects were instructed to keep head movements to a minimum. Ear restraints and foam pads, placed tightly between the forehead and the RF coil contributed further to suppress head motion.

Hardware

Measurements were performed using three nearly identical whole-body scanners, operating at field strengths of 1.5 T (Siemens Avanto), 3 T (Siemens Trio) and 4 T (Siemens/Bruker MedSpec). The scanners have identical software platforms except for different SYNGO version numbers and very similar hardware. All three gradient coils had maximum field strengths of 40 mT/m on each axis. At 1.5 and 3 T, an RF

body coil with very homogeneous B_1-field distribution over the head was used for RF transmit and 12-element, phased-array head coils for signal detection. At 4 T, a composite transmit/receive head coil was used, consisting of a birdcage coil for transmit and an eight-element phased-array coil for signal detection.

Sequences

Quantitative methods were used for the mapping of three relaxation times (T_1, T_2, T_2^*) and the magnetisation density; the latter can be normalised to represent the water content by insertion of a water probe in the FOV. Since the inhomogeneity of the RF field is one of the limiting factors for the accuracy of quantitative methods, B_1 mapping was also performed. The method employed for T_1, T_2^* and water mapping follows the one described in Ref. [12].

Briefly, T_1 mapping was performed using TAPIR, a sequence based on the Look–Locker method. Schematically, the sequence can be depicted as:

$$90^\circ - \tau\,(\text{delay}) - 180^\circ - \text{spoil} - \{\{\{\alpha\text{-module multi-echo readout}\}\ \text{multi-slice acquisition}\} - \text{multi-time points acquisition}\} - \text{spoil}.$$

The spin system is prepared by the sequence of two non-selective (square) pulses with flip angles 90° and 180° respectively, separated by a delay τ. The delay τ is sufficiently large to allow full dephasing of transverse magnetisation created by the 90° pulse. Any transverse magnetisation left after the inversion pulse is removed by means of spoiler gradients in all three directions. Following the inversion pulse, the spin system is repeatedly sampled in a Look–Locker type acquisition scheme by the application of the slice selective (3-lobed sinc) α-pulses, interleaving readout of different slices and time points. In order to accelerate the filling of k-space and, therefore, reduce the acquisition time of the sequence, multiple echoes (number given by the EPI-factor) are read after each α-pulse. The acquired echoes are used to fill different segments of k-space by interleaving blip gradients in phase-encode direction resulting in a k-space with, in our case, five segments. The duration of an α-pulse module is TR, and the repetition time for each slice is TR × number of slices. After the acquisition of the last gradient echo for each slice and each time point, the remaining transverse magnetisation is dephased by means of spoiler gradients. After the acquisition of all time points and all slices, the whole process in then repeated for the next set of lines in k-space.

Detailed information on the sequence and fitting procedure can be found in Refs. [9–13].

Inversion efficiency mapping was performed using exactly the same signal readout module as for TAPIR but without looping over time points. The sequence, called TAPIRIE (TAPIR inversion efficiency) can be depicted as:

$$90^\circ - \tau\,(\text{delay}) - \{180^\circ - \text{spoil} - 180^\circ\} - \text{spoil} - \text{TAPIR multi-slice acquisition}.$$

The sequence was repeated twice for each phase-encode line, once with and once without the combination of two inversion pulses enclosed in parentheses. During reconstruction, data were reordered to produce two separate images for each slice. The ratios of the pixel intensities of these two sets of images reflect the (in)efficiency of the inversion pulse, and were subsequently used during fitting of the dataset (see Sect. Data processing). The same slices and acquisition parameters were used as for TAPIR, with the difference that only one time point was acquired, and the matrix size was 64 instead of 256 in the read-out direction (same phase encode reduction factor) resulting in a 16-times larger voxel size.

T_2^* mapping was performed with a multi-slice, multi-echo, gradient echo sequence in a variant named QUTE [14,15]. A number of equidistant echoes (no. of time points) were acquired, starting at TE and separated by echo space (notations of Table 1). Separate k-spaces were acquired for each echo, and images corresponding to each echo time were reconstructed.

A multi-slice, multi-echo T_2 mapping sequence based on the CPMG method was used for the study of the distribution of transversal relaxation times. A number of equidistant echoes (no. of time points) were acquired starting at TE and separated by TE (notations of Table 1). The sequence (Siemens nomenclature: SE_MC) was included in the standard software distribution provided by the manufacturer (Siemens Medical Solutions, Erlangen, Germany).

A cylindrical probe of 18 mm inner diameter and 12 cm length containing $MnCl_2$-doped water was included in the FOV for calibration of the water content; the $MnCl_2$ content was adjusted such that the relaxation time of the probe was close to the T_1 values found in the brain. The temperature of this probe was measured with an optical sensor.

In addition to the quantitative protocols, a 3D, T_1-weighted sequence (MP-RAGE) was used for anatomical characterisation of the volunteers.

Sequence parameters

In order to attain comparable accuracy at all three fields, the parameters of the sequences were varied at each field. An additional constraint was the demand to keep the total measurement time to around 1 h. The total acquisition time for each field amounted to 1 h, 15 min. Table 1 summarises the main parameters of the quantitative sequences. The pertinent parameters of the MP-RAGE sequence included: TI = 900 ms, TR = 1,670 ms, TE = 2.72 ms, 9° flip angle, field-of-view

Table 1 Sequence parameters of the quantitative sequences used in the present study, for each field strength

	1.5 T	3 T	4 T
TAPIR[a]			
TR (ms)	20	15	15
TE (ms)	3.59	3.20	2.50
TI (ms)	10	8	10
τ (ms)	2,000	2,000	2,000
Time points	16	16	20
EPI factor	5	5	5
α (°)	50°	50°	40°
BW (Hz/pixel)	455	815	700
QUTE[b]			
TR (ms)	112	112	100
TE (ms)	4.58	4.58	4.30
Echo space (ms)	3.4	3.4	2.8
Time points	30	30	32
Flip angle (°)	90°	90°	90°
BW (Hz/pixel)	320	320	399
SE_MC[c]			
TR (ms)	5,200	4,000	4,240
TE (ms)	13.5	13.5	17.5
Time points	20	20	16
Flip angle (°)	90°/180°	90°/180°	90°/180°
BW (Hz/pixel)	160	160	355

[a] TAPIR: volume comprises 41 slices of 2 mm thickness, acquired in three separate measurements with: 14 slices with 300% slice thickness gap, 13 slices with 300% gap, 14 slices with 100% gap between slices, respectively. The matrix size was 256 × 192, the FOV 256 mm × 192 mm, and the spatial resolution 1 mm × 1 mm × 2 mm. The saturation recovery, occurring within a time τ between the non-selective 90° pulse and the 180° non-selective inversion pulse ensures that the same amount of magnetisation is available for every phase encoding step. The listed TR value corresponds to the duration of an α-pulse module; the TR for each slice is TR × number of slices. TE is the echo time of the first echo of the gradient read-out. A number of "EPI factor" echoes are collected and used to fill the k-space for each slice with "EPI factor" segments. A number of "time points" are acquired along the inversion recovery curve for each slice

[b] QUTE: volume comprises 55 slices of 2 mm thickness acquired in two separate measurements with: 28 slices with 100% slice thickness gap and 27 slices with 100% gap between slices. The matrix size was 256 × 192, the FOV 256 mm × 192 mm, and the spatial resolution 1 mm × 1 mm × 2 mm. The multiple echo acquisitions consisted of "time points" number of echoes, starting at TE and spaced by echo space

[c] SE_MC: volume comprises 27 slices of 2 mm thickness acquired in two separate measurements with: 14 slices with 100% slice thickness gap and 13 slices with 100% gap between slices. The matrix size was 256 × 192, the FOV 256 mm × 192 mm, and the spatial resolution 1 mm × 1 mm × 2 mm. A partial Fourier factor of 5/8 was used to speed up the acquisition process. The multiple echo acquisitions consisted of "time points" number of echoes, starting at TE and spaced by TE

(FOV) = 166 × 256 mm^2, matrix size = 208 × 320 (3 and 4 T) or 168 × 256 (1.5 T), 224 coronal slices with 1 mm thickness.

Validation of the methodology

The relaxation times obtained with TAPIR were validated against spectroscopic measurements on tubes containing solutions with different relaxation times due to varying concentrations of Gd, as described in Ref. [9]. Furthermore, results obtained with TAPIR and an inversion-prepared, spin-echo sequence with long TR and varying TI were also compared. The T_2 values obtained with SE_MC and T_2^* values obtained with QUTE were compared to results of single-voxel spectroscopy on a multi-compartment spherical phantom containing solutions with different concentrations of $MnCl_2$. The agreement between the fast mapping sequences and the other imaging or spectroscopic data was found to be very good and is shown in Fig. 1 for T_1 validation at 3 and 4 T; similar results were obtained for T_2 and T_2^* validation.

Brain coverage

In so far as other constraints such as measurement time allowed, this study was designed to achieve nearly complete brain coverage with as high a spatial resolution as possible. Since the different mapping sequences were not equally fast and were subject to different constraints regarding brain coverage (temporal accuracy for TAPIR, SAR limitations for SE_MC), a compromise had to be found between brain coverage, measurement time, and the quantitative power of the methodology for each sequence.

Using the AutoAlign facility of the SYNGO software and the possibility to transfer parameters between the 3 T Trio and 1.5 T Avanto systems using a common database, we acquired the slices in very nearly identical positions with respect to the volunteer's head at 1.5 and 3 T. The replication of this positioning at 4 T using AutoAlign was reasonably close, but not better than manual repositioning of the slices. The different performance of the AutoAlign on the different scanners was probably due to the different software versions (3 T—most up-to-date, 4 T—oldest software version).

The spatial resolution of all acquisitions was 1 mm × 1 mm in-plane with a 2 mm slice thickness. In order to avoid cross-talk effects, a gap of 100% of the slice thickness (2 mm) was kept between slices of any single acquisition. Practically whole brain coverage was achieved with QUTE using two sets of interleaved slices, resulting in a total of 55 (28 + 27) slices. From this volume, a subset of 41 slices was measured with TAPIR, using three sets of slices (14 + 13 + 14). A subset of 27 slices, of those covered by both TAPIR and QUTE, was also measured with SE_MC using two interleaved sets of slices (14 + 13). Thus, the largest contiguous volume simultaneously covered by all three sequences consisted of 27 slices of 2 mm thickness and included the basal ganglia. The largest volume covered by any quantitative sequence amounted to 55 slices of 2 mm thickness and included practically the

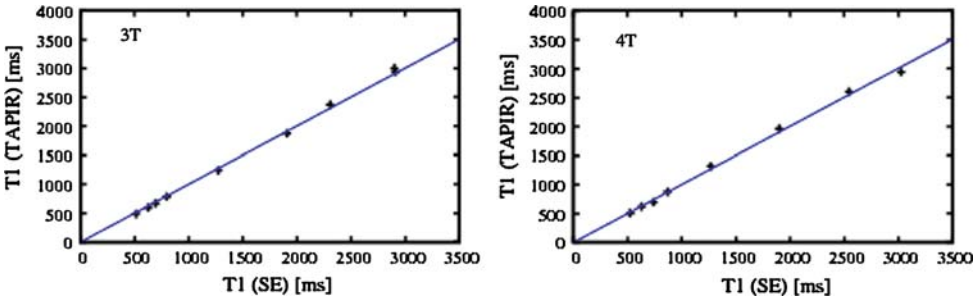

Fig. 1 Validation of T_1 quantitative measurements at 3 and 4 T. Results obtained with the fast mapping sequence TAPIR are compared with results obtained with a single-echo, inversion prepared spin-echo sequence (IR-SE). The *line* represents the best fit to the data

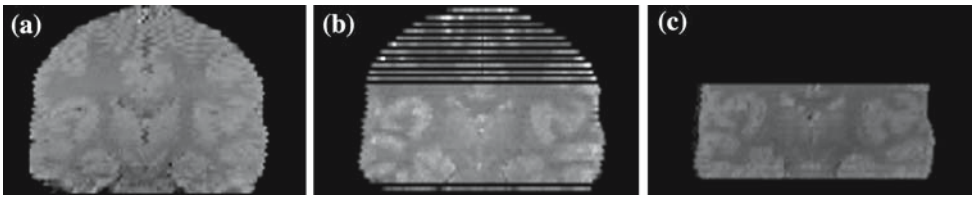

Fig. 2 Coronal reslice of the volumes acquired with QUTE, TAPIR and SE_MC, showing the extent of brain coverage with each sequence. The slice thickness was 2 mm; the gaps between slices, seen in the volume covered by TAPIR, are also 2 mm

whole cerebrum and about a quarter of the cerebellum. The data were acquired in an axial orientation. In Fig. 2 a coronal reslice of the volumes acquired with the three different quantitative sequences is shown illustrating the different extents of brain coverage achieved. A 3D whole-brain acquisition with higher spatial resolution of either 1 mm isotropic (at 1.5 T) or $0.8 \times 0.8 \times 1$ mm (at 3 and 4 T) was performed with MP-RAGE.

Data processing

A Java-based software package developed in-house was used for the computation of the relaxation and magnetisation density maps. Mono-exponential fits were performed to the experimental T_1, T_2 and T_2^* inversion recovery or attenuation curves, respectively. All fits were performed on magnitude data. In order to account for the possibility of having non-exponential T_2^* decays in the regions affected by significant field inhomogeneities [16], a polynomial extrapolation to the zero of time was performed for the voxels where the exponential fit was detected to be poor [12]. For these voxels, the T_2^* parameter was fitted to the later time points, where the decay was well approximated by an exponential [12].

The multiple-echo spin-echo data were fit to the expression $S(t) = A\exp(-t/T_2) + B$, where A is a function of M_0, the equilibrium magnetisation density and B is a constant. For QUTE and SE_MC, the effective value of M_0 extracted from the fits includes T_1 effects due to finite TR as well as B_1 inhomogeneity effects.

In the case of inversion recovery, despite the presence of a large number of voxels where partial volume effects might be expected, and the large number of time points acquired (16), a mono-exponential fit proved to be more robust than a fit using the sum of two exponentials; a mono-exponential fit was consequently used in all cases.

The signal equations and the method used to fit the TAPIR data are the ones given in Ref. [11]. Briefly, one can describe the evolution of the signal with time after inversion as

$$S(t) = A + B\exp(-t/T_1^*),$$

where $1/T_1^* = 1/T_1 - \ln(\cos\alpha)/TR$, A is a function of M_0, T_1, TR and α and B is a function of M_0, T_1, TR, α and K the efficiency of the inversion pulse. K is determined experimentally using the inversion efficiency mapping described in Sect. "Sequences", and the signal is fitted to the above formula with M_0, T_1 and α as fit parameters. Due to the finite value of the echo time of the gradient echo read-out, the effective M_0 extracted by the fit contains a T_2^* contribution, but the B_1 inhomogeneity effects should be eliminated if the fit converged properly.

As described in Ref. [12], by combining the effective magnetisation densities extracted with QUTE and TAPIR with the appropriate T_1, T_2^* and B_1 corrections, and using the water probe for normalisation, the absolute water content of the brain can be calculated.

Based on the 55-slice contiguous volume acquired with QUTE at the shortest echo time, skull removal was performed using the brain extraction tool of FSL (http://www.fmrib.ox.ac.uk/fsl/) [17,18] and a brain mask was created. All the remaining data processing was performed using Matlab (MATLAB V7.0, Release 14. The Mathworks Inc., Natick/MA, USA) and ImageJ (ImageJ 1.36b, National Institutes of Health, USA).

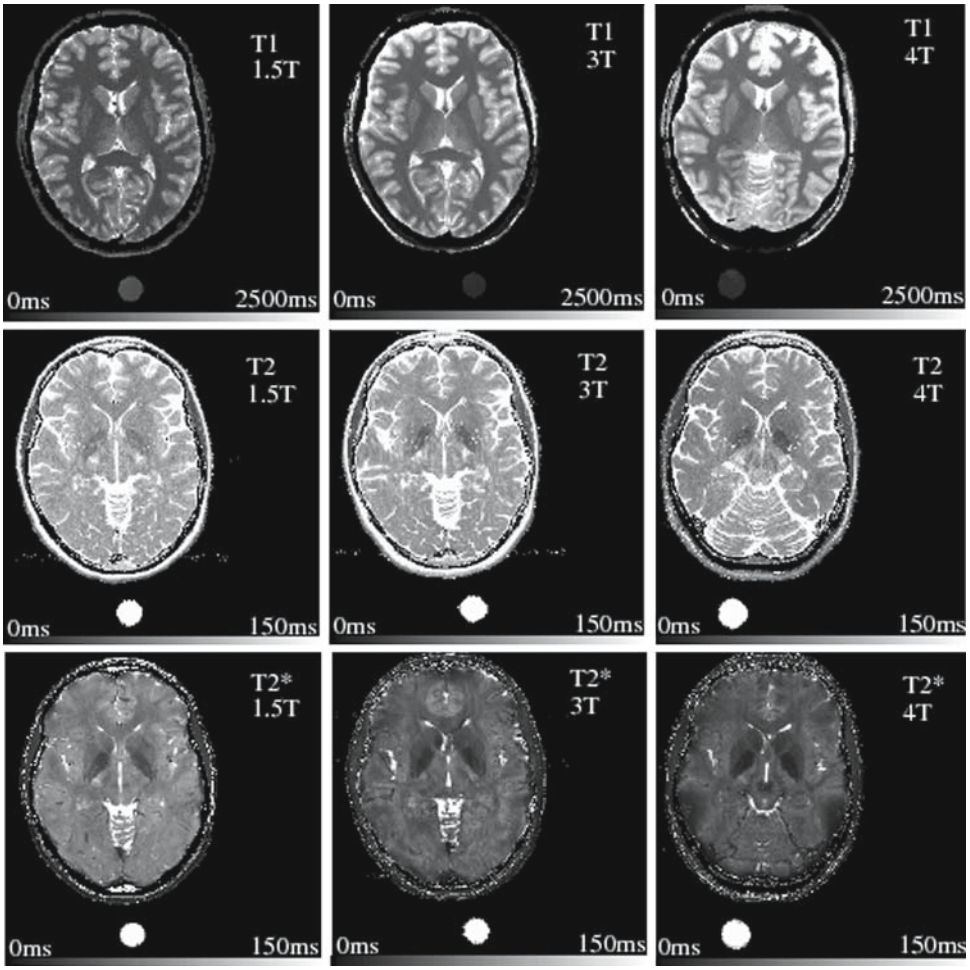

Fig. 3 Maps of the three relaxation times, T_1, T_2 and T_2^*, obtained from a volunteer at 1.5, 3 and 4 T. For each relaxation parameter, the scale is the same across fields and is: 0–2,500 ms for T_1 and 0–150 ms for T_2 and T_2^*. The selected slices are nearly identical at 1.5 and 3 T, and the closest match at 4 T

The fitted relaxation times and magnetisation density maps for each relaxation parameter were separately assembled in volumes of 55 slices. For the T_1 and T_2 acquisitions, the elements of the 3D matrix for which no data were acquired were assigned a value of zero. The brain mask was applied to all these volumes.

Histograms of the T_1 distribution were created for the 41 slices for which T_1 maps were produced, separately for each slice as well as for the whole volume. The summed histogram for each volunteer is thus representative for the whole brain. The number of bins was 256 in all cases. A multi-component fit of the summed distribution was performed, using a superposition of two, three or four Gaussians. Each Gaussian was characterised by its centroid, full-width at half-maximum (FWHM), and maximum value. Segmentation of the brain in white and grey matter was performed based on the T_1 properties of the two types of tissue. Using the T_1-based segmentation, we investigated M_0, T_2 and T_2^* properties separately for white and grey matter.

Results

Validation

The comparison between T_1 values obtained with TAPIR and values obtained with an inversion recovery (IR)-prepared spin-echo sequence with TR of 5 s is shown in Fig. 1. The data were obtained on a multi-compartment phantom filled with water doped with different concentrations of Gd. The agreement is very good, especially for the range of T_1 values relevant for in vivo brain tissue; the coefficients of proportionality are 1.014 ± 0.007 at 3 T and 1.002 ± 0.011 at 4 T. The validation of the methodology at 1.5 T has already been described in previous publications [9–13].

Maps

Longitudinal (T_1) and transversal (T_2 and T_2^*) relaxation maps for a representative volunteer and slice are shown in Fig. 3 for all three field strengths. In addition to the relaxation

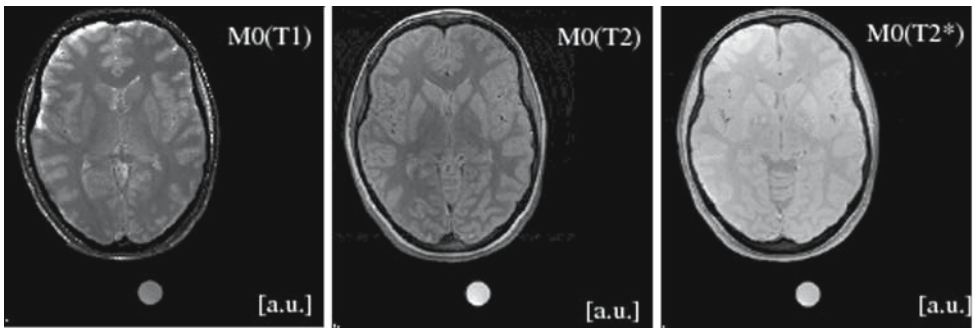

Fig. 4 Maps of the uncorrected magnetisation density (signal intensity at TE = 0), obtained from a voxel-by-voxel mono-exponential fit to the T_1, T_2 and T_2^* data. The maps were all acquired at 3 T and correspond to the same volunteer and slices as the ones of Fig. 3. M0 is given in arbitrary units

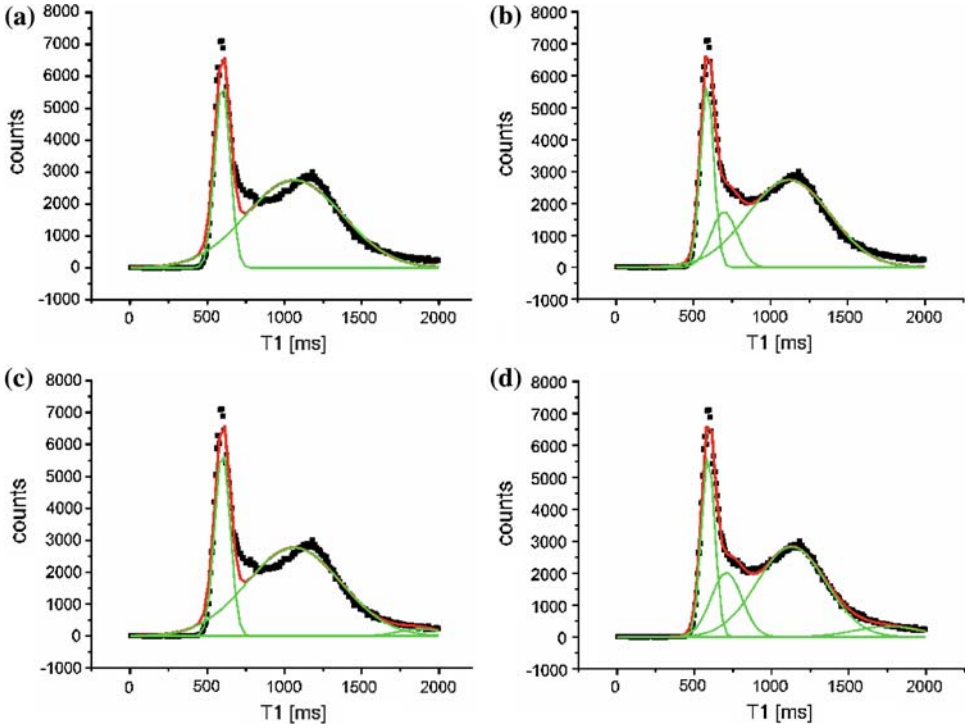

Fig. 5 Whole-brain T_1 histograms for a single volunteer. Data were acquired at 1.5 T. Segments **a**–**d** show multi-Gaussian fits to the data using either 2 (part a: WM + GM), 3 (part b: WM + WM/GM + GM), 3 (part c: WM + GM + GM/CSF) or 4 (WM + WM/GM + GM + GM/CSF) Gaussian distributions. The *red line* represents the best fit to the data, and the *green lines* correspond to each different Gaussian distribution

times, "magnetisation density" maps were produced from each type of relaxation experiment by extrapolating the fitted signal intensity TE = 0 ms (for SE_MC and QUTE) and from the three-parameter (M0, T_1 and α) fit for TAPIR. These maps are shown in Fig. 4.

T_1 distribution

The histogram of T_1 values, including all measured slices, is exemplified in Fig. 5 for one volunteer, with data acquired at 1.5 T. Different decompositions of the histogram are compared: two peaks only, corresponding to the two main "humps"; three peaks including an additional Gaussian between the two main structures; three peaks including an additional Gaussian at T_1 values larger than the ones for the second Gaussian; and four peaks, including all the previous structures. The results of a three-Gaussian decomposition of the T_1 histogram, including the two main "humps" and an additional structure between them, are presented in Fig. 6 for all three fields. The data of Figs. 5 and 6 were acquired on the same volunteer. Table 2 lists values of T_1 in selected anatomical structures.

Segmentation

Segmentation of the white and grey matter was performed following visual inspection of the T_1 maps, separately for every field. The limits chosen for white matter were: 450–875 ms (1.5 T); 550–950 ms (3 T); and 600–1,150 ms (4 T). Similarly, the limits for grey matter were: 876–1800 ms (1.5 T); 951–2,100 ms (3 T); and 1151–2,200 ms (4 T). Based on the T_1 segmentation, it was possible to investigate the characteristic behaviour of the T_2^*, T_2 and M_0 values for the white and grey matter. The whole-brain histograms of these

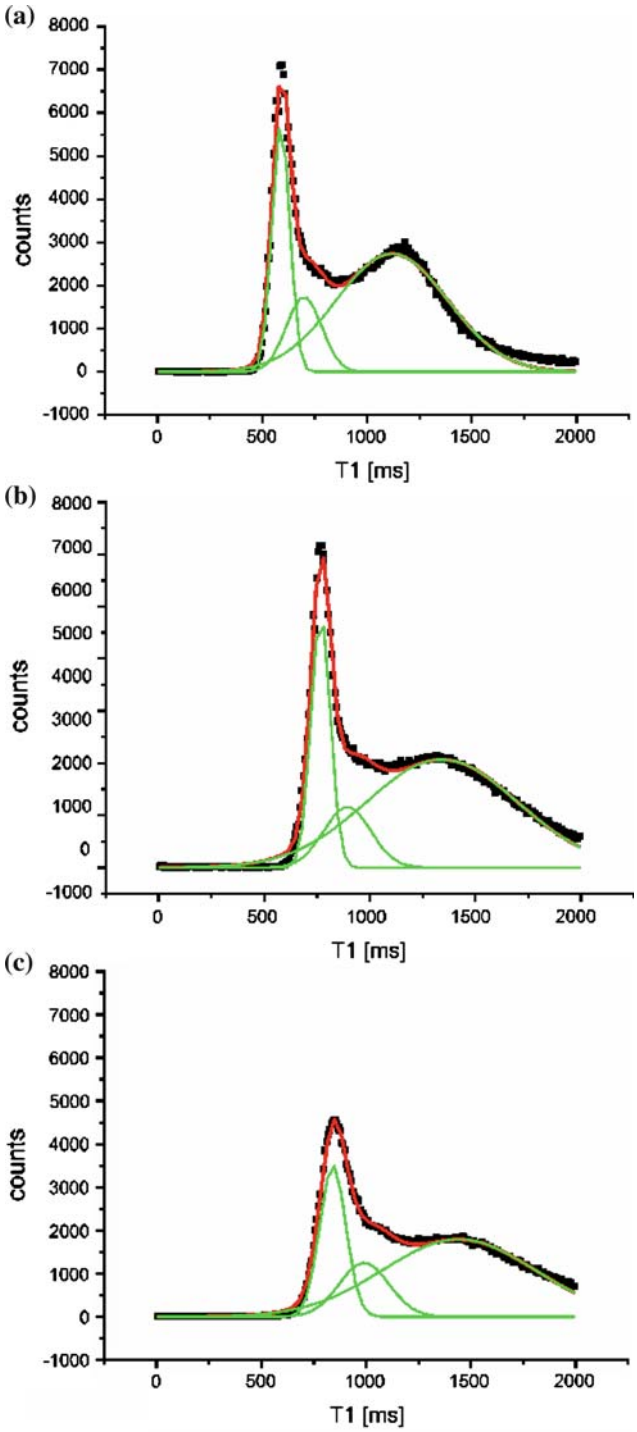

Fig. 6 Decomposition of T_1 histograms at 1.5 T (**a**), 3 T (**b**) and 4 T (**c**) using three Gaussian distributions. The two most intense components correspond largely to white matter (1, WM) and grey matter (3, GM + GM/CSF), whilst the additional component contains a mixture of contributions from white matter voxels, voxels at the border between white and grey matter, and voxels from the deep grey matter. The *red line* represents the best fit to the data, and the *green lines* correspond to each different Gaussian distribution

quantities do not show such distinctive features as the T_1 histogram, and segmentation in white and grey matter would not be possible based on T_2 and T_2^* information only. This point is exemplified in Fig. 7, which shows the T_2^* and T_2 histograms as a function of field strength for a representative volunteer.

Discussion

At the time when this study was initiated (October 2006), in vivo relaxation times obtained at more than two different field strengths on the same volunteer and measured with the same method (sequence, manufacturer) were not available in the literature. In the meantime, results on the field dependence of T_1 values of the in vivo brain, at five different field strengths (0.2, 1, 1.5, 4 and 7 T), have been published [19]. Rooney et al. [19] used a single, 5 mm thick slice that was measured for three volunteers using different scanners (hardware and software) at different MR centres. Systematic differences in relaxation times can arise because of differences in the acquisition sequence and/or processing techniques. However, most modern MRI instruments have comparable performances and identical acquisition sequences can be coded across different manufacturers (and can be verified by oscilloscope). Exact details regarding hardware and operating software can be made largely irrelevant as long as appropriate care is taken in sequence coding. Rooney et al. [19] used different scanners (hardware and software), but made an impressive effort to implement identical pulse sequences (and processing code) across all magnetic field strengths.

The work presented here distinguishes itself from the above-mentioned study in a number of important ways: first, we have measured T_1, T_2, and T_2^* on 12 volunteers; second, by employing multi-slice acquisitions, we have covered nearly the whole brain for T_1 and overlapping slabs for the other two maps; third, the implementation of identical methods was facilitated by the use of nearly the same scanner software; and finally, our slice thickness is 2 mm which offers significantly more immunity from the deleteriousness of partial volume effects. The different RF setup at 4 T constituted the biggest hardware difference between the three scanners, and the different performance of the AutoAlign at 4 T the biggest software difference. The 1.5 and 3 T scanners can be considered as differing only in the field strength and being otherwise identical.

A disadvantage of this study is that we have measured at 3 field strengths and not 5 as have Rooney et al. [19]. Furthermore, the range of the magnetic fields used here is modest (1.5–4 T; a factor of 2.7) compared to the quoted study (0.2–7 T; a factor of 35).

The T_1 values determined in this work compare well with values published by other groups at the field strengths we have used (see Table 2). The comparison with the study by Rooney et al. [19], in which T_1 values were measured with

Table 2 T_1 values in selected anatomical regions

Tissue	Time (ms)	1.5 T	3.0 T	4.0 T
Globus pallidus	T_1	746 [19[b]]	1,043 [24]	1,143 [19[b]]
		880[a] [20[b]]	**888 (31)**	1,210[a] [20[b]]
		733 (20)		**933 (33)**
Red nuclei	T_1	835[a] [20[b]]	**833 (66)**	1,020[a] [20[b]]
		674 (43)		**825 (53)**
Putamen	T_1	981 [19[b]]		1,446 [19[b]]
		1,060[a] [20[b]]	1,337 [24]	1,700[a] [20[b]]
		919 [21]	**1,140 (41)**	1,372 [25]
		942 [22]		1,289 [27]
		996 (34)		**1,296 (46)**
Genu of corpus callosum	T_1	625 [22]		
		700 [23]	**720 (24)**	**800 (23)**
		569 [11]		
		558 (28)		
Splenium of corpus callosum	T_1	672 [22]		
		692 [23]	**730 (23)**	1,155[a] [20[b]]
		568 [11]		**816 (28)**
		581 (17)		
Thalamus	T_1	972 [19[b]]	1,218 [24]	1,452 [19[b]]
		1,150[a] [20[b]]	**1,016 (40)**	1,650[a] [20[b]]
		814 [21]		1,215 [27]
		839 [22]		**1,055 (41)**
		872 (31)		
Caudate nuclei	T_1	1,083 [19[b]]	1,483 [24]	1,509 [19[b]]
		1,033 [21]	1,271 [26]	1,458 [25]
		1,023 [22]	**1,226 (53)**	1,425 [27]
		1,056 (37)		**1,353 (70)**

The values from the present study, shown in bold, are averaged over the right and left hemispheres. The mean value and the SD, given inside parentheses, are calculated over the 12 volunteers. At each field, data from the literature are shown for comparison. The references [11,19–27] are indicated inside the square brackets

[a] Case study

[b] Study conducted at more than one field strength

the same method at several fields, shows better agreement for the values acquired at 1.5 T than for those measured at 4 T. The latter are approximately 150 ms lower in our work than those of Ref. [19].

A possible explanation of differences between T_1 values determined with sequences based on the same method (Look–Locker) and employing similar corrections and fit methods might arise from different magnetisation transfer (MT) effects and thus different influences on the T_1 times. As has been noted very recently [28,29], T_1 values determined with an inversion-prepared turbo spin echo (TSE) sequence with a moderate number of slabs (5 or 6) show substantial (20–30%) shortening compared, for example, with values obtained with TAPIR. This is most probably due to magnetisation transfer effects in a sequence (TSE) which employs many 180° pulses. In our case, besides using pulses with a much smaller flip angle, the number of slices used in any TAPIR measurement is rather small (13 or 14), but larger than the single slice acquired by Rooney et al. [19]. However, pronounced magnetisation transfer effects on T_1 values would also lead to a slice dependence of the relaxation times even in a homogeneous phantom, if its structure allows for MT effects, and we have not noticed this in TAPIR acquisitions.

In contrast with the comparison of T_1 values for selected regions, the mean T_1 values for the whole of the GM extracted in this work, 1,127 (27) ms at 1.5 T and 1,466 (29) ms at 4 T, are higher that the value reported in Fig. 6 of Ref. [19] of 1,000 ms at 1.5 T and 1,400 ms at 4 T. This is most probably due to the fact that the discussion in Rooney et al. [19] is based on data from a single slice, where a significant fraction of the grey matter was concentrated in the basal ganglia, with values lower than those of the cortical grey matter. It is to be noted that whilst there is usually high consistency between T_1 values measured in different volunteers in a given study, the differences between T_1 values measured with different methods, using different hardware and manufacturers, are usually quite large. This makes it difficult to study the field dependence of relaxation times using values published by

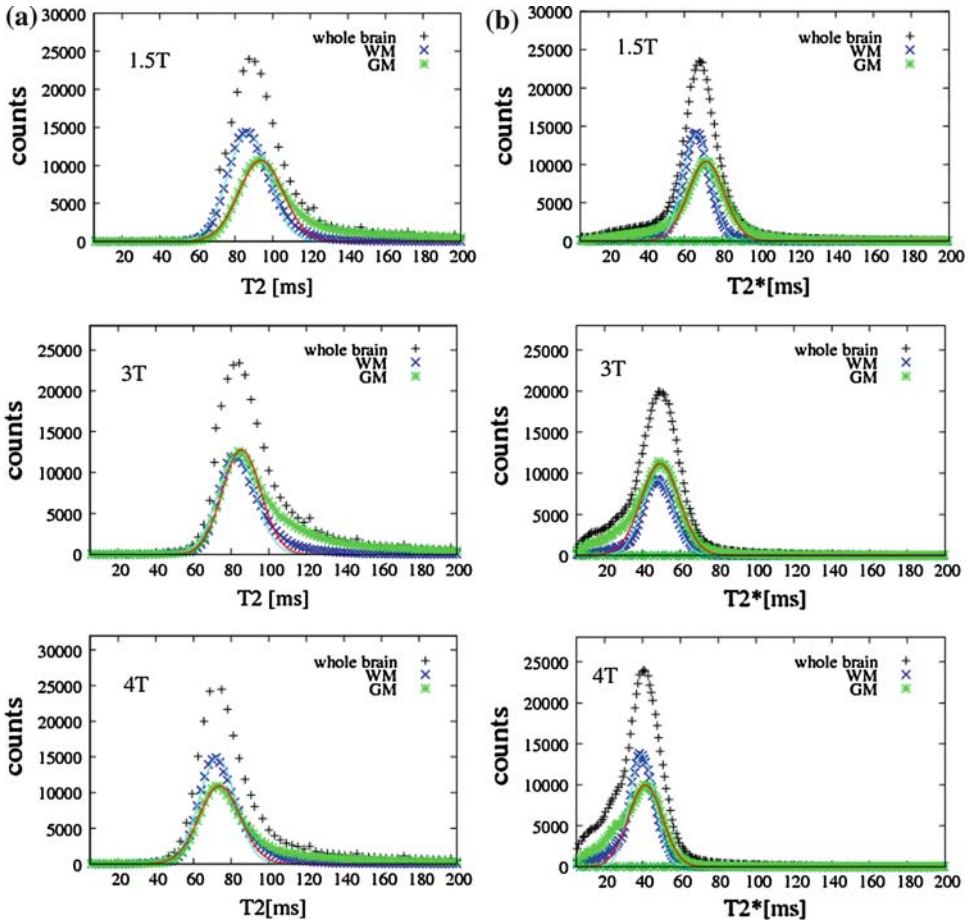

Fig. 7 Histograms of T_2 (**a**) and T_2^* (**b**) distributions at three different fields for the whole volume acquired on one of the volunteers. The decomposition in white and grey matter is based on the corresponding T_1 segmentation at the given field strength. The curves correspond to Gaussian distributions

different groups. Additionally, values across studies are often reported from selected, but non-identical regions only.

A clear strength of our study lies in the fact that besides the use of the same mapping method and data evaluation software, we have employed scanners which are practically identical except for the field strength and the RF coil. The volunteers were measured at all three field strengths within a very short time (2 weeks on average), making any significant changes in the intrinsic properties of the brain unlikely. Furthermore, we have achieved extensive brain coverage (41 slices for T_1 mapping) with a high spatial resolution for a quantitative method ($1 \times 1 \times 2$ mm). The former aspect ensures that the conclusions regarding the behaviour of the T_1 distribution in the brain is not biased by the use of a single slice, with very specific anatomy. To exemplify this point, we show in Fig. 8 the comparison between the histogram obtained from one slice through the basal ganglia and the histogram from the whole data set acquired at 1.5 T for a single volunteer. The latter aspect minimises the partial volume effects and allows for a better study of the properties of distinct tissue types.

The different RF coils employed at the different fields give rise to different B_1 distributions. The B_1 inhomogeneity of

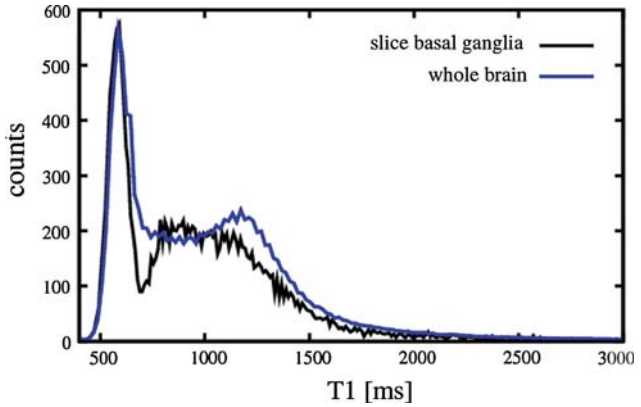

Fig. 8 Comparison between T_1 histograms from: **a** a slice through the basal ganglia, and **b** the whole volume acquired with TAPIR (41 slices). Both histograms are normalised to unity. *Top* to *bottom*: 1.5–4 T

the body coils used for transmit at 1.5 and 3 T was small over the volume of the brain, but the birdcage coil used for transmit at 4 T displayed a substantial RF field inhomogeneity. Figure 9 compares the inversion efficiency maps extracted for selected slices with high RF inhomogeneity at 4 T (part b) and 3 T (part e). The factor displayed is the absolute value

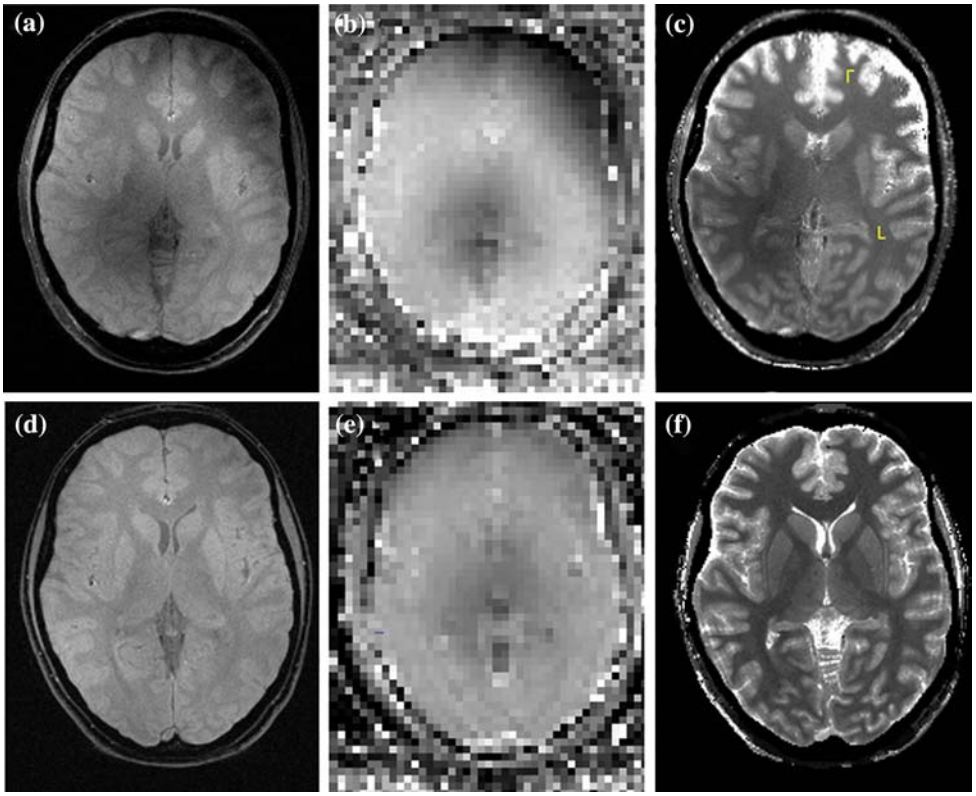

Fig. 9 Effect of the B_1 inhomogeneity on the raw data and quantitative maps with increasing field and different RF configurations. *Top row:* data acquired at 4 T; *bottom row:* data acquired at 3 T. Parts (**a**) and (**d**) show slices acquired with TAPIR (last time point on the saturation recovery curve) in a region of inhomogeneous RF distribution at 4 T (**a**) or 3 T (**d**). Parts (**b**) and (**e**) show the measured distribution of the cosine of the inversion pulse. The scale is 0.3–1.2 in part (**b**) and 0.5–1.2 in part (**e**). Parts (**c**) and (**f**) show the calculated T_1 maps. It is seen that for the regions of very high RF inhomogeneity at 4 T several cases of fit misconvergence appear, whereas at 3 T the effect of coil inhomogeneity is not noticeable in the quantitative map. However, even at 4 T, when the fit converges properly, it gives similar T_1 values for the white matter in the region of high inhomogeneity as in a homogeneous region (ROIs on part (**c**)

of the cosine of the inversion pulse (nominal value is 1 for 180°), and the scale ranges from 0.3 to 1.2 in part (b) and 0.5 to 1.2 in part (e). At 4 T, besides the not very pronounced signal drop-out in the centre of the brain encountered at high fields, the left side of the frontal region was affected by large inhomogeneities, because the inversion pulse was close to 135°. The effect of the B_1 inhomogeneity on the raw data acquired with TAPIR at the last time point sampled on the saturation recovery curve is exemplified in part (a) for 4 T and (d) for 3 T. It can be seen that the SNR values improve with field strength. Comparing the SNR values for a region in the genu of corpus callosum among fields gives values of 8.3 at 1.5 T, 8.9 at 3 T and 9.3 at 4 T. The errors in the T_1 fit due to reduced SNR of the raw images should therefore, diminish with increasing field. However, the very strong, inhomogeneity of the RF coil gives rise to pixels of clear fit mis-convergence in the frontal region at 4 T, and a larger spread of the fitted value when the fit does converge. Regarding the absolute T_1 values, the mean values over the two white matter ROIs shown on part (c) for 4 T, one in a strongly inhomogeneous, one in a homogeneous region, are practically identical.

T_1 histograms

The well-known fact that T_1 contrast between white and grey matter in the healthy in vivo brain is the highest of the 3 MR parameters measured here is well substantiated by the histograms. Two well separated features, a narrow peak and a broader "hump" can be easily distinguished at all fields employed in the present study (see Fig. 6). However, a fit of the histograms using two Gaussian distributions does not deliver satisfactory results (see Fig. 5a).

The three-Gaussian decomposition of the T_1 histograms (Figs. 5c, 6) reproduces the data well. A natural assignment of the peaks would be, in the order of increasing T_1: white matter, voxels at the border between white and grey matter, and grey matter. However, inspection of the T_1 maps shows that the first and second peaks are both largely characteristic of the white matter. Some voxels with T_1 values belonging

to the second peak originate in the deep grey matter; some others belong to regions in which CSF, grey and white matter all overlap within one voxel. For each field, the T_1 values which separate the grey and white matter for the purpose of segmentation, chosen after careful inspection of the data, are close to the point of intersection between the sum of the first two Gaussian distributions and the third one.

A large number of voxels with grey matter content are affected by partial volume effects. Since our data have higher in-plane resolution than slice thickness, and the sulcal landscape varies very rapidly in the brain, most of the voxels affected by partial volume effect can be expected to be at the border between grey matter and CSF. The values of T_1 for CSF was found to be practically independent of the field strength and amount to 4.3 s [19], and voxels affected by partial volume effects can display T_1 values ranging from the lower end of the grey matter T_1 distribution up to the CSF value. This is an extremely broad interval, and the histograms show no clear structure in the region of long T_1 values. Another reason for the lack of a clear CSF peak is that the T_1 values for CSF measured with TAPIR are not really meaningful. The pulsatile motion of the CSF is a problem for TAPIR since the high temporal resolution with which TAPIR samples the recovery curve is at the expense of building up the images line by line over several TR intervals. Also, the time interval for which the recovery curve has been sampled (number of slices × number of time points × TR) was optimised for brain tissue relaxation times and is too short to allow for a good fit for components with very long T_1.

A three-Gaussian fit of T_1 histograms at 1.5 T using WM, GM and GM-CSF was employed by Suzuki et al. [30]. However, in the region between WM and GM the fit of their data also significantly underestimates the observed distribution of T_1 values.

In our case, adding another Gaussian to the 3-peak decomposition, to additionally characterise the border between grey matter and CSF, makes the fit unstable in many cases. The variation with field strength of the characteristics of different components becomes less reliable. We have, therefore, chosen the robust three-component fit (WM, WM-GM, GM) to characterise the whole-brain T_1 distribution and compare its features between volunteers and fields.

The limits chosen for segmentation at 1.5 T are slightly different from those of Neeb et al. [13], who employed the same mapping method. The main difference is in the cut-off for grey matter (1,800 ms in the present study, vs. 1,150 ms in Ref. [13]). The significantly higher resolution in our study, of $1 \times 1 \times 2$ mm compared to $1 \times 1 \times 5$ mm in [13], is the main reason for this difference. The segmentation values chosen by Suzuki et al. [30] agree well with our value when half the voxels corresponding to the GM-CSF border are assigned to grey matter.

We note here that because of the lack of appropriate criteria for "good segmentation", all segmentation limits are quite arbitrary. The segmentation limits need to be established not only for each field separately, but also, in principle, for each volunteer. Since age and sex play a role in the characteristics of the T_1 distributions, the border between the values corresponding to WM and GM are likely to show dependence on the same factors. However, especially for studies with a large number of volunteers, manual segmentation can become prohibitive in terms of workload. In addition, its subjectivity introduces a source of errors.

With this caveat in mind, the limits chosen for segmentation of the brain in WM and GM at different fields should be considered only as a starting point. They have been determined for the volunteer whose T_2 and T_2^* data are shown in Sect. "Transversal relaxation times". For different volunteers, these limits can well vary by several tens ms.

Field dependence of T_1 values

In Fig. 10a we present the centroids of the three Gaussian peaks, which fit the T_1 histograms, as a function of field strength. Individual data from four separate volunteers are shown together with the mean values and SD obtained from the full collective of 12 volunteers. Figure 10b shows similar data for the width w of the Gaussian peaks ($w = 2\sigma$, approximately 0.849 full width at half maximum FWHM). Peaks 1 and 2 describe the white matter, whilst peak 3 is assigned to the grey matter. Besides the clear increase in the T_1 values with field, it is also noteworthy that the values for WM and GM are still diverging at 4 T, albeit slowly. The pure T_1 "contrast-to-signal" ratio between white and grey matter can be calculated using ROIs in the genu of corpus callosum (GCC) and the caudate nucleus (CN). With the data listed in Table 2, the contrast-to-signal ratio $[T_1(\mathrm{CN}) - T_1(\mathrm{GCC})]/[T_1(\mathrm{CN}) + T_1(\mathrm{GCC})]$ is approximately constant with field and has a value of around 0.28 (0.31 at 1.5 T and 0.26 at both 3 and 4 T).

As seen in Fig. 10b, the widths of the T_1 distributions also increase with field, more prominently so for the grey matter. The distinctness of the WM and the GM distributions reduces with increasing field strength; this is partly due to the T_1 values of the deep grey matter which increase less rapidly than the cortical ones. The increased T_1 heterogeneity of the cortical brain tissue provides greater discrimination power of T_1 contrast at high fields. We mention that part of the broadening of the T_1 distribution for grey matter at 4 T might well be due to the strong RF field inhomogeneity depicted in Fig. 9. As seen in part (c), the T_1 values deduced for the grey matter in regions of extremely strong field inhomogeneity are longer than those for the GM in other regions. Despite the fact that the efficiency of the inversion pulse was measured experimentally and included in the signal expression

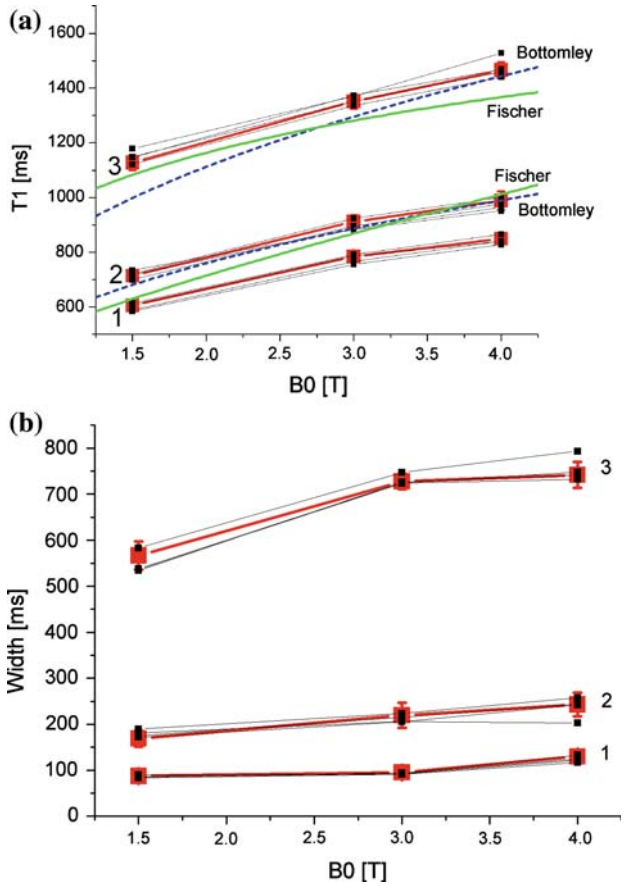

Fig. 10 Field dependence of the characteristics of the three peaks corresponding to the three-Gaussian decomposition of the experimental T_1 histograms. Part (**a**): centroids; part (**b**): widths. Data for four different volunteers are shown to illustrate the similarity of the field dependence between subjects. The mean value and SD calculated over the 12 volunteers are shown in *red*. The field dependence of the centroids is compared to predictions using empirical formulae from Bottomley et al. [1] and Fischer et al. [2]

for TAPIR, and the fit should correct for the remaining pulse inhomogeneity effects, this did not succeed in a few regions were the RF inhomogeneities were too strong. The effect is also present, but less pronounced, for regions in the centre of the brain, for example the basal ganglia. For these regions the RF inhomogeneity contributes to produce a larger spread in the fitted value and will slightly increase the width of the corresponding T_1 distribution.

The field dependence of the longitudinal relaxation time has been fitted using ex vivo NMR dispersion data by Bottomley [1] and Fischer et al. [2]. Bottomley used the simple empirical formula:

$$T_1 = A\nu^B, \tag{1}$$

where ν is the NMR frequency and A and B fit parameters. The values of the two parameters have been fitted to in vivo data recently by Rooney et al. [19]; we use those parameters in our comparison. In Fig. 10a, we plot the curve $T_1 = A\nu^B$ (dotted blue line) with the parameters: $A = 0.00071$ and $B = 0.382$ for the white matter and $A = 0.00116$ and $B = 0.376$ for the grey matter [19]. The agreement is reasonably good. The difference in the values for the grey matter most probably arises from the fact that the fit parameters extracted in Ref. [19] are based on T_1 values for the putamen only whereas the centroid of our distribution represents the whole of grey matter (predominantly cortical), with longer T_1 values. For the white matter, the predicted values agree very well with the value of the centroid of the second peak. The majority of the white matter voxels (more than half) are nevertheless described by the first peak and their relaxation times are thus shorter than the predicted value. The shape of the field dependence of the white matter, which is the same for the centroids of peaks 1 and 2 (WM and WM-GM), is well predicted. However, given that the predicted field dependence of the grey matter is steeper than the field dependence shown by our data, the divergence of the T_1 values with field seems over predicted using the parameters derived from Rooney et al. [19].

The continuous green line in Fig. 10a represents the formula proposed by Fischer et al. [2], that is:

$$1/T_1 = 1/T_1, w + D + A/[1 + (f/f_c)^\beta], \tag{2}$$

with the parameters given in Table 2 of Fischer et al. [2]. For the sake of completeness, however, we reproduce the parameters here: $1/T_1$,w, relaxation rate of pure water $= 0.23\,s^{-1}$ (at 37°C); $D[s-1] = 521.38$ (WM), 0.105 (GM); $A[s-1] = 18.25$ (WM), 11.66 (GM); f_c[MHz] $= 0.165$ (WM), 0.059 (GM); $\beta = 0.291$ (WM), 0.42 (GM). This expression has the advantage over Bottomley's formula that the relaxation rate does not diverge at high fields, but converges towards a value approximately equal to that of pure water, and the relaxation times are finite at zero field strength.

Fischer's formula offers a slightly better overall agreement with our data. This is not surprising, since it contains more fit parameters than Bottomley's formula. However, the variation of the relaxation times with field strength is overestimated for the white matter and underestimated for the grey matter, leading to an extrapolated convergence of the T_1 values at higher fields, which is not substantiated by our data.

Due to the small range of magnetic fields investigated in this study, it is not possible to assess based on our data which of the functions is better suited to model the T_1 behaviour as a function of magnetic field over a large range of fields. However, the comparison of the predictions of formula [1] with our data up to 4 T shows an overestimation, while formula [2] underestimates the behaviour of T_1 with field strength. An overestimation of the difference in the T_1 values of white and grey matter offered by formula [1] at 7 T is also present in the data of Ref. [19]. The discrepancy between real values

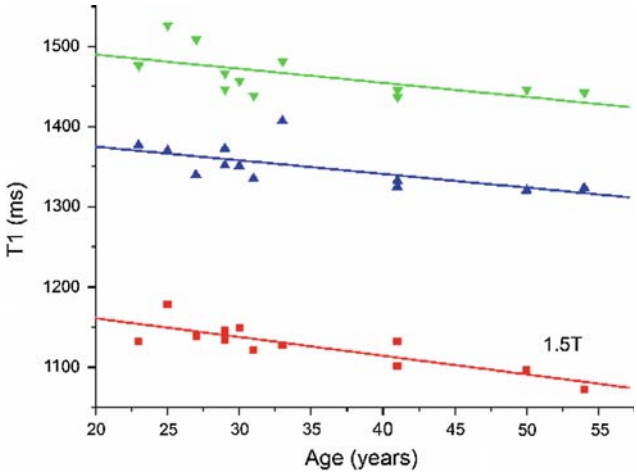

Fig. 11 Age dependence of the centroid of the Gaussian distribution corresponding to the grey matter. The behaviour for each field is shown separately

of T_1 at 9.4 and 11.7 T and those predicted by either formula [1] or [2] might be substantial.

Age dependence of T_1 values

The age dependence of the centroids obtained from the three-Gaussian decomposition of the T_1 histograms was investigated. A clear variation of the position of the GM peak with age was observed and is shown in Fig. 11: T_1 of GM was found to decrease linearly with age. The results were consistent across fields, and the slope of the T_1 (GM) dependence on field was found to be slightly lower for 3 T ($-1.7(2)$) and 4 T ($-1.8(2)$) than for 1.5 T ($-2.3(3)$). In all cases, the probability that the correlation was due to chance was $P < 0.05$. No clear correlation with age was observed for the centroids attributable to WM. At the three fields, the P-value for a linear fit was between 0.16 and 0.97. The result concerning the decrease of the T_1 of GM with age is in agreement with the findings of Suzuki et al. [30] at 1.5 T. In our case, a linear expression, instead of the quadratic one used by [30], was found to perform better perhaps due to the more limited age range of the volunteers in our study (23–54 years, compared to 23–88 years [30]).

A strong correlation of the T_1 of WM with age was found by Suzuki et al. whereas our data, corroborated by the results of Neeb et al. [13] (see below), show no such behaviour. An important difference between the two studies, which might well explain the discrepancy, was that the collective included in the study of Suzuki et al. consisted of patients affected by different neurological diseases, whereas our data were acquired on healthy volunteers.

Andersen [31] reported a constant increase of the T_1 averaged over manually chosen regions-of-interest (ROI) in the frontal and parieto-occipital white matter between 20 and 60 years. However, based on the ROI analysis in frontal white matter, Cho et al. [32] found an increase in longitudinal relaxation time starting only in the 6th decade of life, but no variation for subjects aged 20–50 years. This result is similar to our findings for the white matter distribution in the whole brain. It is, however, difficult to compare regional and global results, since the WM in specific regions might show different behaviour from that averaged over the whole brain.

The main contributions to T_1 relaxation in brain tissue arise from the macromolecular content of the tissue, as well as iron content [19]. The largest quantitative survey of the behaviour of human brain iron content with age was performed with chemical and histopathological methods by Hallgren and Sourander [33]. Their results show that, in addition to a substantial heterogeneity of the grey matter with respect to accumulations of non-haemin iron, the age dependence of the accumulation is also heterogeneous. For the whole brain, the most pronounced variation takes place between birth and 20 years of age. The variation of iron content thereafter is strongly reduced in magnitude. Iron content in parts of the cortex (for example, the motor cortex) increases with age up to about 50 years of age. For the putamen and caudate nucleus, iron accumulation continues until 50–60 years. For many other parts of the brain, including globus pallidus and frontal white matter, however, no notable increase is noticed after 30 years of age [33]. In the thalamus, a rise of iron content up to around 35 years is observed followed by a decrease. If the variation of T_1 observed here with age reflects the average variation of the iron content over the whole GM, the differences noticed in the slope of the dependence of T_1 with field might reflect relaxivity changes due to iron (decreases slightly with increasing field).

However, the stronger influence on the longitudinal relaxation rate is due to macromolecular content, which in turn influences the water content of the tissue [Bottomley et al. 1984]. Mansfield and Morris [34] noticed a linear relationship between T_1 and water content, which they describe by $T_1 = 7.94w - 5.16$ for non-adipose tissue, with w being the fractional water content. As seen from the large slope, and as discussed by Bottomley et al. [1], the changes in water content which produce significant changes in T_1 are quite marginal. This led to the inference that macromolecular composition and structure is probably the determinant factor in this correlation, playing a major role in the functionality of tissue, including its water content, as well as a major role in the NMR relaxation times.

Neeb et al. [13] investigated the age dependence of the water content of the white and grey matter in the whole brain, also taking into account the gender dependence. They found a clear (and quadratic) decrease in the male GM water content starting in the 6th decade of life, and a clear (and linear) decrease in the female GM water content over the whole age interval studied (20–70 years). Judging from Fig. 3 of

Table 3 Centroid (x_0) and width (FWHM) of the Gaussian distributions which best correspond to the WM and GM T_2 and T_2^* distributions

B(T)	1.5 T[a]	3 T[a]	4 T[a]
T_2: WM: x_0 (ms)	87.0 (1)	83.9 (2)	72.6 (2)
WM: FWHM (ms)	25.8 (3)	25.0 (6)	22.8 (5)
GM: x_0 (ms)	93.8 (1)	85.6 (2)	74.0 (2)
GM: FWHM (ms)	27.8 (4)	26.1 (4)	25.9 (5)
T_2^*: WM: x_0 (ms)	66.5 (5)	48.8 (4)	39.8 (4)
WM: FWHM (ms)	17.0 (6)	19.8 (6)	15.5 (7)
GM: x_0 (ms)	71.5 (8)	49.3 (8)	41.5 (8)
GM: FWHM (ms)	22.5 (6)	24 (1)	21.0 (7)

The segmentation of the brain in white and grey matter is based on T_1 segmentation. The errors given in parentheses represent the fit uncertainty. The data are for one representative volunteer
[a] Values from a single volunteer

Ref. [13], the behaviour of male GM water content with age over the interval included in this study (23–54 years) can be considered constant. No age or gender specific changes were observed for the white matter. These findings are in very good agreement with the behaviour of T_1 values found in the present study, with a mixed male and female collective, as can be expected due to the strong correlation between T_1 and water content. The influence of field strength on this relationship requires further investigation.

Transversal relaxation times

As seen in Fig. 7, the field dependence of the transversal relaxation times is less pronounced than that of the longitudinal relaxation time, but nevertheless noticeable. The parameters of the Gaussian distributions which represent the best fit to the experimental T_2 distributions for WM and GM, respectively, at different fields, are given in Table 3.

The difference in the T_2 and especially T_2^* values for the bulk of white and grey matter becomes very small after 3 T. The absolute values of the bulk relaxation rates increase with field somewhat more rapidly than a linear dependence.

Whilst field independence of the T_2 relaxation time can be expected theoretically [5], the contribution from diffusion of water molecules in inhomogeneous magnetic fields influences the measured relaxation times. This contribution introduces a field dependent component via the susceptibility gradients [35]. In addition, the effective transversal relaxation time, T_2^*, is also affected by dephasing produced by static field inhomogeneities. This component can also be strongly field dependent, if the effect is due to susceptibility inhomogeneities. The field dependence of the contribution to the relaxation rate caused by diffusion in susceptibility gradients is quadratic [36,37].

Another field-dependent contribution arises from relaxation caused by ferritin deposits in the brain. In contrast to the diffusion-mediated mechanism, the field dependence in this case is linear [38].

It is difficult, using relaxation data acquired at only three field values to reliably separate linear and quadratic contributions to the relaxation rates. However, in regions where the relaxation is dominated by ferritin deposits as, for example, in the globus pallidus, the relaxation rates show a field dependence which is different from that of regions where no significant ferritin deposits are to be expected (data not shown).

Besides the shortening of relaxation times with increasing field strength, seen in Fig. 7, one notable effect is the appearance of a "shoulder" in the short relaxation times region of the T_2^* distribution. This is due predominantly to regions with strong susceptibility gradients (as in the frontal regions) or iron deposits (e.g., globus pallidus or putamen).

As mentioned in Sect. "Data processing", the T_2^* values were extracted from mono-exponential fits to the relaxation curves. It is known that the presence of intra-voxel gradients can result in a non-exponential decay of the FID from the respective voxel [16].

In such a case, the fitted T_2^* value is an underestimate of the relaxation time.

However, even at 4 T, the experimental decay curves were found to be close to exponential in most regions. In these regions, the relaxation rates R_2, R_2^* and $R_2' = R_2^* - R_2$, and their field dependence can give information about the iron content in brain tissue.

A limitation of the T_2 and T_2^* component of this study is that results are presented for a single volunteer. Although we feel these results are representative of the T_2 and T_2 behavioural trends of a larger sample, the conclusions must be considered preliminary. We expect to publish a more complete study of T_2 and T_2^* behaviour from the complete cohort of 12 volunteers in the near future.

Conclusions

Longitudinal and transversal relaxation times have been determined at three different field strengths in the in vivo human brain, using very similar whole-body scanners and near identical sequences. The quantitative sequences were validated against spectroscopic and imaging standards, with very good agreement. In vivo results were obtained on eight male and four female volunteers, aged between 23 and 54 years. This paper focuses on the results from longitudinal relaxation time mapping, and exemplifies the results obtained for transversal relaxation times on one volunteer only. Practically whole brain coverage was obtained for the T_2^* maps (55 slices), close to whole brain for the T_1 maps (a subset of 41 slices) and around half of the brain volume (27 slices) was investigated regarding its T_2 properties. We have, thus, extracted information about the whole-brain

behaviour of the relaxation times, in order to avoid conclusions based on specific structures only. In addition to the extended brain coverage, high resolution was achieved for quantitative sequences: 1 mm × 1 mm in plane, and 2 mm slice thickness. Partial volume effects were thus kept to a minimum.

The global distribution of T_1 values was investigated. A three-Gaussian decomposition was found to best reproduce the experimental T_1 distributions for all volunteers at all three field strengths. The peaks correspond, in the order of increasing T_1 values, largely to white matter, border between white and grey matter (with contributions from, among others, the basal ganglia), and grey matter. The latter peak partly includes voxels at the border between grey matter and CSF. Besides the well-documented increase of the T_1 relaxation time with the field strength, visual inspection of the whole-brain T_1 histograms shows that the separation between the peaks corresponding to white matter only (peak no. 1) and grey matter (peak no. 3) is becoming less distinct with increasing field. This is due to a large extent to the fact that the field dependence of T_1 in the basal ganglia is less pronounced than that of cortical grey matter. The values corresponding to the basal ganglia increasingly fill the gap between the T_1 values of white and cortical grey matter.

We have investigated the field dependence of the centroids and widths of the three Gaussians which characterise the whole-brain distribution of T_1 values. The overall field dependence is quite well reproduced by both Bottomley's formula [1] with parameters adjusted by Rooney et al. [19], and by Fischer's formula [2] with the original parameters. However, the separation between the experimental centroids corresponding to white and grey matter is either overestimated (Bottomley's formula with Rooney's parameters) or underestimated (Fischer's formula) towards high fields. This separation is a matter of concern regarding the usefulness of very high fields for in vivo brain imaging. Based on our data and data from the literature, it seems very unlikely that the T_1 contrast between white and grey matter will disappear even at the highest fields where human in vivo imaging is planned (11.7 T). The increasing spread in the T_1 values of grey matter with increasing field strength, and to a more moderate extent, those of white matter, are likely to allow for better differentiation of brain regions which are microscopically different. We note that increased RF field inhomogeneities at 4 T might also have contributed to the observed increase in the width of the T_1 distributions, most pronouncedly so for the grey matter.

We have further investigated the age dependence of the centroids of the three peaks identified in the global distribution of T_1 values. No correlation with age was identified for the white matter T_1 values. In contrast, a clear dependence of the T_1 of grey matter on age was noticed: the T_1 values decrease linearly with increasing age over the interval investigated here (23–54 years). A slight dependence of the proportionality constant on field was noticed. However, the limited size of our group of volunteers did not allow us to study the age dependence separately for males and females, whereas a study of the brain water content indicates that the behaviour might be different [13]. In order to investigate the field dependence of the proportionality constant which describes the age dependence of T_1 values, further investigation of the T_1 behaviour with age should be performed at different field strengths with larger groups of volunteers and covering a more extended age interval.

The brain tissue was segmented in white and grey matter based on T_1 values. Based on this segmentation, it was possible to investigate the behaviour of the T_2 and T_2^* values of white and grey matter separately. The bulk values of the relaxation rates were found to increase with field.

By combining the information obtained for all three relaxation times, the study of the field dependence of these NMR properties is expected to allow for better differentiation between regions which are structurally different, provide a better insight into the microscopic structure of the brain and the molecular substrate of its function.

Scanners with similar hardware and software as the three scanners used here are becoming available at the ultra-high fields of 7 and 9.4 T. In future work, it would be very desirable to complement our data with values of the relaxation times at these fields obtained for the whole brain with the same mapping method.

Acknowledgments The authors are grateful to Mrs. C. Kemper and Mrs. B. Elghahwagi for help with the selection and coordination of volunteers. Enlightening discussions with Dr. H. Neeb at various stages of this work are gratefully acknowledged. This research was supported by grants from the Bundesministerium fuer Bildung und Forschung (BMBF).

References

1. Bottomley PA, Foster TH, Argersinger RE, Pfeifer LM (1984) A review of normal tissue hydrogen NMR relaxation times and relaxation mechanisms from 1–100 MHz: dependence on tissue type, NMR frequency, temperature, species, excision, and age. Med Phys 11: 425–448
2. Fischer HW, Rinck PA, Van Haverbeke Y, Muller RN (1990) Nuclear relaxation of human brain gray and white matter: analysis of field dependence and implications for MRI. Magn Reson Med 16: 317–334
3. Li TQ, van Gelderen P, Merkle H, Talagala L, Koretsky AP, Duyn J (2006) Extensive heterogeneity in white matter intensity in high-resolution T_2^*-weighted MRI of the human brain at 7.0 T. NeuroImage 32: 1032–1040
4. Duyn JH, van Gelderen P, Li TQ, de Zwart JA, Koretsky AP, Fukunaga M (2007) High-field MRI of brain cortical substructure based on signal phase. PNAS 104: 11796–11801
5. Bloembergen N, Purcell EM, Pound RV (1947) Relaxation effects in nuclear magnetic resonance absorption. Phys Rev 73: 679–715

6. Koenig S (1996) Molecular basis of magnetic relaxation of water protons of tissue. Acad Radiol 3: 597–605
7. Bryant RG, Mendelson DA, Coolbaugh Lester C (1991) The magnetic field dependence of proton spin relaxation in tissues. Magn Reson Med 21: 117–126
8. Halle B, Denisov VP, Venu K (1999) Multinuclear relaxation dispersion studies of protein hydration. Biol Magn Reson 17: 419–449
9. Shah NJ, Zaitsev M, Steinhoff S, Zilles K (2001) A new method for fast multislice T_1 mapping. NeuroImage 14: 1175–1185
10. Steinhoff S, Zaitsev M, Zilles K, Shah NJ (2001) Fast T_1 mapping with volume coverage. Magn Reson Med 46: 131–140
11. Zaitsev M, Steinhoff S, Shah NJ (2003) Error reduction and parameter optimization of the TAPIR method for fast T_1 mapping. Magn Reson Med 49: 1121–1132
12. Neeb H, Zilles K, Shah NJ (2006) A new method for fast quantitative mapping of absolute water content in vivo. NeuroImage 31: 1156–1168
13. Neeb H, Zilles K, Shah NJ (2006) Fully-automated detection of cerebral water content changes: study of age- and gender-related H2O patters with quantitative MRI. NeuroImage 29: 910–922
14. Shah NJ, Zaitsev M, Steinhoff S, Wiese S, Zilles K (2000) Development of sequences for fMRI: keyhole imaging and relaxation time mapping. http://eenc.uni-leipzig.de/Shah.pdf
15. Dierkes T, Neeb H, Shah NJ (2004) Distortion correction in echo-planar imaging and quantitative T_2^* mapping. Proceedings of the international workshop on quantitation in biomedical imaging with PET and MRI. Int Congr Ser 1265: 181–185
16. Dahnke H and Schaeffter T (2005) Limits of detection of SPIO at 3T using T_2^* relaxometry. Magn Reson Med 53:1202–1206
17. Smith SM (2002) Fast robust automated brain extraction. Human Brain Map 17(3): 143–155
18. Smith SM, Jenkinson M, Woolrich MW, Beckmann CF, Behrens TEJ, Johansen-Berg H, Bannister PR, De Luca M, Drobnjak I, Flitney DE, Niazy R, Saunders J, Vickers J, Zhang Y, De Stefano N, Brady JM, Matthews PM (2004) Advances in functional and structural MR image analysis and implementation as FSL. NeuroImage 23: 208–219
19. Rooney WD, Johnson G, Li X, Cohen ER, Kim S-G, Ugurbil K, Springer CSJr (2007) Magnetic field and tissue dependencies of human brain longitudinal 1H2O relaxation in vivo. Magn Reson Med 57: 308–318
20. Schenk JF (1995) Brain iron by magnetic resonance: T_2 at different field strengths. J Neurol sci 134: 10–18
21. Kingsley PB, Ogg RJ, Reddick WE, Steen RG (1998) Correction of errors caused by imperfect inversion pulses in MR imaging measurement of T_1 relaxation times. Magn Reson Imag 16: 1049–1055
22. Steen RG, Reddick WE, Ogg RJ (2000) More than meets the eye: significant regional heterogeneity in human cortical T_1. Magn Reson Imag 18: 361–368
23. Vavasour IM, Clark CM, Li DK, Mackay AL (2006) Reproducibility and reliability of MR measurements in white matter: clinical implications. Neuroimage 32: 637–642
24. Gelman N, Ewing JR, Gorell JM, Spickler EM, Solomon EG (2001) Interregional variation of longitudinal relaxation rates in human brain at 3.0 T: relation to estimated iron and water contents. Magn Reson Med 45: 71–79
25. Jezzard P, Duewell S, Balaban RS (1996) MR relaxation times in human brain: measurement at 4 T. Radiology 199: 773–779
26. Lin C, Bernstein MA, Huston J, Fein SB (2001) In vivo and in vitro measurements of T_1 relaxation at 3.0 T. Proc 9th Meeting of the Intl Soc Mag Reson Med 9:1391
27. Kim SG, Hu XP, Ugurbil K (1994) Accurate T_1 determination from inversion-recovery images-application to human brain at 4-Tesla. Magn Reson Med 31: 445–449
28. Meara SJ, Barker GJ (2007) Impact of incidental magnetization transfer effects on inversion recovery sequences that use a fast spin-echo readout. Magn Reson Med 58(4): 825–829
29. Turner R, Oros-Peusquens AM, Romanzetti S, Zilles K and Shah NJ. Optimised in-vivo visualisation of cortical structures in the human brain at 3T using IR-TSE. Magn Reson Imag 2008, in print
30. Suzuki S, Sakai O, Jara H (2006) Combined volumetric T_1, T_2, and secular-T_2 quantitative MRI of the brain: age-related changes: preliminary results. Magn Reson Imag 24: 877–887
31. Andersen C (1997) In vivo estimation of water content in cerebral white matter of brain tumour patients and normal individuals: towards a quantitative brain oedema definition. Acta Neurochir. (Wien) 139: 249–256
32. Cho S, Jones D, Reddick WE, Ogg RJ, Steen RG (1997) Establishing norms for age-related changes in proton T_1 of human brain tissue in vivo. Magn Reson Imag 15: 1133–1143
33. Hallgren P, Sourander B (1958) The effect of age on the non-haemian iron in the human brain. J Neurochem 3: 41–51
34. Mansfield P, Morris D (1982) NMR imaging in biomedicine. Academic, New York, pp 10–32
35. Bartha R, Michaeli S, Merkle H, Adriany G, Andersen P, Chen W, Ugurbil K, Garwood M (2002) In vivo 1H2O T2+ measurement in the human occipital lobe at 4T and 7T by Carr–Purcell MRI: detection of microscopic susceptibility contrast. Magn Reson Med 47: 742–750
36. Majumdar S, Gore JC (1998) Studies of diffusion in random fields produced by variations in susceptibility. J Magn Reson 78: 41–55
37. Kennan RP, Zhong J, Gore JC (1994) Intravascular susceptibility contrast mechanisms in tissues. Magn Reson Med 31: 9–21
38. Gossuin Y, Muller RN, Gillis P (2004) Relaxation induced by ferritin: a better understanding for an improved MRI iron quantification. NMR Biomed 17:427–432
39. Rooney WD, Li X, Springer CS, Telang FW, Coyle PK, Caparelli E, Ernst T, Chang L. Age and sex: effects on brain properties assessed by 1H2OT1 histograms. In: Proceedings of the 11th Annual Meeting of ISMRM,Toronto, Canada, 2003 (Abstract 1087)